JOURNAL OF PROPULSION AND POWER
Vol. 10, No. 5, Sept.–Oct. 1994

Computation of Shock-Induced Combustion Using a Detailed Methane-Air Mechanism

Shaye Yungster* and Martin J. Rabinowitz†
NASA Lewis Research Center, Cleveland, Ohio 44135

The shock-induced combustion of methane-air mixtures in hypersonic flows is investigated using a new reaction mechanism consisting of 19 reacting species and 52 elementary reactions. This reduced model is derived from a full kinetic mechanism via the detailed reduction technique. Zero-dimensional computations of several shock-tube experiments are presented first. The computed values for ignition delay and flame speed are in close agreement with experimental data and with results obtained using a full mechanism. The new reaction mechanism is then combined with a fully implicit Navier-Stokes CFD code to simulate two-dimensional and axisymmetric shock-induced combustion experiments of stoichiometric methane-air mixtures at a Mach number of $M = 6.61$. Good agreement with the experiments is obtained. Furthermore, it is shown that previous calculations were unable to accurately predict this type of flow due to their use of severely limited reduced chemical mechanisms. Finally, applications to the ram accelerator concept are also presented, based on a novel double-ramp configuration.

Nomenclature

A = pre-exponential factor in rate coefficient
a^*, b^*, c^* = constants, Eq. (13)
b = temperature exponent in rate coefficient
d = diameter
e = total energy per unit volume
J = grid Jacobian
K = rate coefficient
K_C = equilibrium constant
M = Mach number
M_i = molecular weight of ith species
n = total number of chemical species
p = pressure
$\dot{Q}_{\max}$ = maximum rate of heat release of any reaction
R = universal gas constant, also radius of cylinder
T = temperature
u = velocity component in x direction
v = velocity component in y direction
w = chemical source term
Y = arbitrary specification of all chemical species
y_i = concentration of species Y_i
ΔH = enthalpy of reaction
$\varepsilon_K, \varepsilon_Q$ = parameters much smaller than unity
η = curvilinear coordinate normal to body surface
Θ = activation temperature in rate coefficient
μ^0 = species standard state Gibbs free energy per mole
ν = stoichiometric coefficient
ξ = curvilinear coordinate along body surface
ρ = density

Subscripts
b = backward
f = forward
i = species index
j = reaction index
∞ = freestream

Superscripts
0 = low pressure limit
∞ = high pressure limit

Introduction

ONE of the main obstacles in the computation of high-speed flows with hydrocarbon combustion has been the lack of reliable reaction mechanisms that are reasonably simple and yet still reproduce experimental observations over a wide range of conditions. Detailed kinetic mechanisms have been developed for the simplest fuel molecules. Oxidation models for methane, e.g., typically consist of 100–250 elementary reactions, and more significantly, they include from 28 to 50 or more species.[1–5] Since the computational cost associated with a given reaction mechanism depends primarily on the number of species included, the use of these models would be prohibitively expensive when combined with existing two- or three-dimensional CFD codes.

As a result, previous computations of high-speed methane airflows, aimed at studying detonation waves and the ram accelerator concept,[6] have used either simplified global and quasiglobal models,[7,8] or mechanisms composed of elementary reactions whose rate parameters are collected from literature recommendations.[8]

Global mechanisms reduce an entire reaction scheme to a small number of usually unrealistic chemical reactions. Quasiglobal models, such as those developed by Westbrook and Dryer,[9] combine a single reaction of fuel and oxidizer with a detailed mechanism for a CO—H_2—O_2 system. These mechanisms were developed mainly for modeling flames. Although they have the potential to reproduce accurately some flame properties such as flammability limits, combustion temperature, and burned gas composition, they generally cannot describe accurately the chemical structure of the flame itself. In shock-induced combustion problems this will translate in an

Presented as Paper 93-1917 at the AIAA/SAE/ASME/ASEE 29th Joint Propulsion Conference, Monterey, CA, June 28–30, 1993; received Aug. 2, 1993; revision received Jan. 10, 1994; accepted for publication Jan. 20, 1994.

*Research Associate, Institute for Computational Mechanics in Propulsion. Member AIAA.
†Physicist, Internal Fluid Mechanics Division.

incorrect prediction of the induction zone. Furthermore, the parameter ranges over which these simplified mechanisms can accurately be applied are rather narrow. A second disadvantage of quasiglobal models is their sensitivity to the numerical models used. These models were developed mainly based on flame speed data. As a result, they depend not only on the rate parameters, but also on thermodynamic and transport properties that may be treated somewhat differently in other codes. Therefore, for use in other codes, it is generally necessary to calibrate the pre-exponential factor in each individual reaction.

On the other hand, mechanisms that are simply a collection of elementary reactions suffer from the following principle:

"A mechanism composed of reactions with best available rate parameters individually is incapable of quantitative predictions when taken as a whole.[1]"

For these mechanisms, in which the individual reactions may have been validated under conditions of chemical isolation, when combined they usually do not reproduce experimental observations accurately. In addition, many plausible reactions are ignored in this approach without first estimating their potential effects, and the general guidelines for reaction model development are violated.[10]

There is therefore a need for a reasonably simple and reliable kinetic mechanism for methane-air combustion in high-speed flows. Several approaches for reducing chemical reacting systems have been suggested and pursued recently by several researchers. They generally include the global reaction method previously mentioned, "response modeling" in which algebraic relationships are developed between model responses and model variables, direct reduction in size of a detailed mechanism, and lumping of chemical systems based on the specific topology of the reaction network. These approaches were recently reviewed and discussed in Ref. 10. Here, we employ the detailed reduction technique to develop a new methane oxidation model that consists of 19 reacting species and 52 elementary reactions. In this approach, no global steps are introduced. Therefore, the reduced mechanism has the potential to give accurate predictions over a wide range of flow conditions, and still be practicable in terms of computational resources. In addition, this mechanism can be implemented into existing CFD codes without the need to modify their basic structure. The main disadvantage of using detailed reduction is that the resulting model is still quite complex, requiring at least an order of magnitude more computational time than the quasiglobal mechanisms. The extra cost is fully justified in the present case, since it is shown that the global models are unable to accurately predict the ignition delay in shock-induced combustion flows.

The reduced methane oxidation model is combined with a fully implicit CFD code to numerically simulate expansion-tube experiments conducted at the French-German ISL Institute[11] aimed at studying ram-accelerator-related combustion phenomena. Results are presented for superdetonative flows of methane-air mixtures around various bodies, and are compared with experimental data and with the computations performed by Soetrisno et al.[8] Applications to an axisymmetric ram accelerator projectile are also presented.

Numerical Formulation

Governing Equations

The computations are conducted using the Navier-Stokes equations for two-dimensional or axisymmetric flow, in which the global continuity equation is replaced by all the species continuity equations. They can be expressed in the following conservation form for a gas containing n species and in general curvilinear coordinates (ξ, η)

$$\frac{\partial \boldsymbol{Q}}{\partial t} + \frac{\partial(\boldsymbol{F} - \boldsymbol{F}_v)}{\partial \xi} + \frac{\partial(\boldsymbol{G} - \boldsymbol{G}_v)}{\partial \eta} + j(\boldsymbol{H} - \boldsymbol{H}_v) = \boldsymbol{W} \quad (1)$$

where

$$\boldsymbol{Q} = J^{-1} \begin{bmatrix} \rho_1 \\ \rho_2 \\ \vdots \\ \rho_n \\ \rho u \\ \rho v \\ e \end{bmatrix} \quad (2)$$

The equations describe two-dimensional flow if $j = 0$, and axisymmetric flow if $j = 1$. The variables are the density of the ith species ρ_i, with $\rho = \Sigma_{i=1}^{n} \rho_i$, the velocity components u and v, and the total energy per unit volume e. The term J denotes the grid Jacobian. $\boldsymbol{F}$ and $\boldsymbol{G}$ are the inviscid flux vectors in the ξ and η directions, respectively. Similarly, $\boldsymbol{F}_v$ and $\boldsymbol{G}_v$ are the viscous fluxes. The terms $\boldsymbol{H}$ and $\boldsymbol{H}_v$ are the axisymmetric source terms, and $\boldsymbol{W}$ is the chemical source term. A detailed description of all the terms appearing in Eq. (1), and of the additional state and constitutive equations needed to close the system can be found in Yungster.[12]

Reaction Model

The methane oxidation mechanism used in this study was developed via the technique of detailed reduction[13] starting from the full mechanism of Frenklach et al.[1] Detailed reduction is a systematic method of reducing large reaction networks while maintaining the accurate prediction of selection combustion characteristics. Usually a kinetic mechanism is developed to predict a range of combustion characteristics (ignition, species profiles, flame velocities, pollutant emission, etc.), many of which are not important for a particular application. For shock-induced combustion calculations, the fate of species that do not contribute significantly to heat release or ignition is unimportant. To test the contribution of various species and reactions two criteria were developed:

$$|K_j| < \varepsilon_K |K_{\text{ref}}| \quad (3)$$

$$|K_j \Delta H_j| < \varepsilon_Q \dot{Q}_{\max} \quad (4)$$

where K_j is the rate of reaction j, K_{ref} is the rate of a reference reaction (usually the rate limiting reaction, in this case the reaction of $H + O_2 \rightleftharpoons OH + O$), ΔH_j is the enthalpy of reaction j, $\dot{Q}_{\max}$ is the maximum heat release per unit time of any reaction, and ε_K and ε_Q are parameters much smaller than unity. The first inequality tests the contribution of each reaction to chain branching (and hence, ignition delay), and the second to heat release. Reactions whose rates, both forward and reverse, satisfy Eqs. (3) and (4) are removed from the mechanism. A series of zero-dimensional calculations was performed with values of ε_K and ε_Q around 0.1 for 11 shock-tube test cases of dilute methane-oxygen matrices. These experimental cases were taken from various sources,[1] and the most reliable and representative ones were used. The shock-tube experiments were simulated with an in-house computer code using the LSODE integrator of Hindmarsh, and using a constant density model.[1] The two criteria given in Eqs. (3) and (4) were evaluated at the point of maximum rate of heat release.

It was found that the complete 33 species, 149 reaction mechanism[1] could be reduced to 19 species and 52 reactions while still maintaining good accuracy. The results are shown in Table 1. The flame velocity for a stoichiometric, 1-atm methane flame was computed using the Sandia burner codes.[1] A flame speed of 39.2 cm/s was obtained, in close agreement with the experimental value (40 cm/s), and with the value obtained with the full mechanism (39.5 cm/s). The reactions for the reduced mechanism and their rate coefficients are listed in Table 2.

Table 1 Ignition delay, μs

IC[a]	Experiment	Full[b]	Reduced[b]
1	268	236 (−12)	245 (−9)
2	46	49 (7)	51 (11)
3	18	22 (22)	23 (28)
4	436	497 (14)	530 (22)
5	99	101 (2)	107 (8)
6	99	97 (−2)	99 (0)
7	1512	1361 (−10)	1378 (−9)
8	550	538 (−2)	546 (−1)
9	226	249 (11)	253 (12)
10	205	187 (−8)	192 (−6)
11	210	241 (15)	255 (21)

[a]See Ref. 1 for details of cases IC1 through IC11.
[b]Percent deviation in parentheses.

Calculation of the Chemical Source Term *W*

The chemical equation for a general elementary reaction j in a gas mixture containing n species can be written as

$$\sum_{s=1}^{n} \nu'_{s,j} Y_s \rightleftharpoons \sum_{s=1}^{n} \nu''_{s,j} Y_s \tag{5}$$

where $\nu'_{s,j}$ and $\nu''_{s,j}$ are the stoichiometric coefficients of reaction j. The rate of change of the concentration of species i in reaction j, denoted as $\dot{y}_{i,j}$, is given by

$$\dot{y}_{i,j} = (\nu''_{i,j} - \nu'_{i,j}) \left[K_{f,j} \prod_{s=1}^{n} y_s^{\nu'_{s,j}} - K_{b,j} \prod_{s=1}^{n} y_s^{\nu''_{s,j}} \right] \tag{6}$$

where y_i is the concentration of species Y_i ($y_i = \rho_i/M_i$). The total rate of change of the concentration of the ith species caused by all of the chemical reactions is

$$\dot{y}_i = \sum_j \dot{y}_{i,j} \tag{7}$$

The components w_i of the chemical source term W are given by

$$w_i = \dot{y}_i M_i \tag{8}$$

The forward-rate coefficients K_f of pressure-independent reactions are calculated from

$$K_{f,j} = A_j T^{b_j} e^{-\Theta_j/T} \tag{9}$$

where T is the temperature, and A_j, b_j, and Θ_j are constants. Note that the dissociation reactions of CH_4, C_2H_5, and C_2H_6 (reactions 33, 48, and 49) are in the falloff region and require special treatment for pressure-dependent rate coefficients. The pressure dependence of these reactions is treated based on the Troe-Golden formalism[1]

$$K_j^0 = A_j^0 T^{b_j^0} e^{-\Theta_j^0/T} \tag{10}$$

$$K_j^\infty = A_j^\infty T^{b_j^\infty} e^{-\Theta_j^\infty/T} \tag{11}$$

$$P_r = \frac{K_j^0 [M]}{K_j^\infty} \tag{12}$$

where K_j^0 and K_j^∞ are the low- and high-pressure limiting rate coefficients, and $[M]$ denotes the concentration of the third body. Note that M has been written within parentheses in Table 2 to indicate that it should not be included in Eq. (6)

$$F_c = a_j^* e^{-b_j^*/T} + (1 - a_j^*) e^{-c_j^*/T} \tag{13}$$

where a^*, b^*, and c^* are constants (given in Table 2):

$$x_t = \frac{1}{1 + (\log P_r)^2} \tag{14}$$

The forward rate coefficients of pressure-dependent reactions are then given by

$$K_{f,j} = K_j^\infty \frac{P_r}{1 + P_r} F_c x_t \tag{15}$$

The rate coefficients of the reverse reactions K_b were determined via equilibrium constants

$$K_{b,j} = \frac{K_{f,j}}{K_{C,j}} \tag{16}$$

where $K_{C,j}$ is the equilibrium constant for the jth reaction, and is given by

$$K_{C,j} = \frac{\exp\left(- \sum_{s=1}^{n} \nu_s \mu_s^0 / RT \right)}{(RT)^{\Delta\nu_s}} \tag{17}$$

where

$$\Delta\nu_s = \sum_{s=1}^{n} \nu_s, \quad \nu_s = \begin{cases} -\nu'_s & \text{for reactants} \\ \nu''_s & \text{for products} \end{cases} \tag{18}$$

Here, R is the universal gas constant, and μ_s^0 is the species standard state Gibbs free energy per mole, which is determined from fourth-order polynomials of temperatures. (The other thermodynamic and transport properties are also computed using polynomial functions of temperature.[14])

Numerical Method

The system of Eq. (1) is solved using a fully implicit finite difference CFD code.[12] It employs an iterative method based on the LU-SSOR implicit factorization scheme,[15] and Yee's second-order total variation diminishing (TVD) differencing scheme.[16] In the present study, a symmetric TVD scheme with a minmod type limiter is used. The viscous terms are evaluated using standard central differences. The full Jacobian of the chemical source term is used, leading to a preconditioner matrix of size $n \times n$ that has to be inverted at every grid point. The structure of the LU-SSOR algorithm allows full vectorization of the CFD code, including the matrix inversion process which is done using Crout's algorithm (without pivoting). The scheme is suitable for steady-state calculations, and can be made time accurate by choosing numerical time steps smaller than the time scale of the transient process of interest. In the present work, only steady state calculations have been performed. Further details about the algorithm can be found in Yungster.[12]

Results

Shock-Induced Combustion

Numerical simulations of two sets of expansion-tube experiments conducted by Srulijes et al.[11] at the French-German ISL Institute are presented. Both cases considered a stoichiometric methane-air mixture at a static pressure $p_\infty = 0.51$ bar, static temperature $T_\infty = 295$ K, and a superdetonative velocity of $U_\infty = 2330$ m/s (Mach number $M = 6.61$). The Chapman-Jouguet detonation speed of the gas mixture under these conditions was computed[11] to be about $D = 1800$ m/s.

The first set of experiments consisted of cylindrical steel rods placed perpendicularly to the flow inside a combustion test chamber. For a fixed flow velocity, the diameter of the rods was progressively reduced down to a lower limit beyond which ignition did not occur. Two pressure transducers mounted on the tube wall, one placed upstream and the other downstream of the rod, recorded the pressure history. The results of this experiment indicated a sharp ignition onset between

Table 2 Methane-air reaction mechanism[a]

No.	Reaction	A	Θ	b
1	$H + O_2 \rightleftharpoons OH + O$	1.59×10^{17}	8,491.28	−0.927
2	$O + H_2 \rightleftharpoons OH + H$	3.87×10^{4}	3,151.16	2.70
3	$OH + H_2 \rightleftharpoons H_2O + H$	2.16×10^{8}	1,725.92	1.51
4	$OH + OH \rightleftharpoons O + H_2O$	2.10×10^{8}	−199.65	1.40
5	$H + H + M \rightleftharpoons H_2 + M$	6.40×10^{17}	0.0	−1.0
6	$H + OH + M \rightleftharpoons H_2O + M$	8.40×10^{21}	0.0	−2.0
7	$H + O_2 + M \rightleftharpoons HO_2 + M$	7.00×10^{17}	0.0	−0.8
8	$HO_2 + H \rightleftharpoons OH + OH$	1.50×10^{14}	505.15	0.0
9	$HO_2 + H \rightleftharpoons H_2 + O_2$	2.50×10^{13}	348.79	0.0
10	$HO_2 + O \rightleftharpoons O_2 + OH$	2.00×10^{13}	0.0	0.0
11	$HO_2 + OH \rightleftharpoons H_2O + O_2$	6.02×10^{13}	0.0	0.0
12	$H_2O_2 + M \rightleftharpoons OH + OH + M$	1.00×10^{17}	22,851.89	0.0
13	$CO + OH \rightleftharpoons CO_2 + H$	1.22×10^{7}	−317.52	1.35
14	$CO + O + M \rightleftharpoons CO_2 + M$	3.01×10^{14}	1,515.44	0.0
15	$CHO + H \rightleftharpoons CO + H_2$	7.23×10^{13}	0.0	0.0
16	$CHO + O \rightleftharpoons CO + OH$	3.00×10^{13}	0.0	0.0
17	$CHO + OH \rightleftharpoons CO + H_2O$	1.00×10^{14}	0.0	0.0
18	$CHO + O_2 \rightleftharpoons CO + HO_2$	4.20×10^{12}	0.0	0.0
19	$CHO + M \rightleftharpoons CO + H + M$	1.86×10^{17}	8,551.42	−1.0
20	$CH_2O + H \rightleftharpoons CHO + H_2$	1.26×10^{8}	1,094.49	1.62
21	$CH_2O + O \rightleftharpoons CHO + OH$	3.50×10^{13}	1,768.01	0.0
22	$CH_2O + OH \rightleftharpoons CHO + H_2O$	7.23×10^{5}	−488.31	2.46
23	$CH_2O + O_2 \rightleftharpoons CHO + HO_2$	1.00×10^{14}	20,085.61	0.0
24	$CH_2O + CH3 \rightleftharpoons CHO + CH4$	8.91×10^{-13}	−481.09	7.4
25	$CH_2O + M \rightleftharpoons CHO + H + M$	5.00×10^{16}	38,487.40	0.0
26	$CH_3 + O \rightleftharpoons CH_2O + H$	8.43×10^{13}	0.0	0.0
27	$CH_3 + OH \rightleftharpoons CH_2O + H_2$	8.00×10^{12}	0.0	0.0
28	$CH_3 + O_2 \rightleftharpoons CH_3O + O$	4.30×10^{13}	15,503.20	0.0
29	$CH_3 + O_2 \rightleftharpoons CH_2O + OH$	5.20×10^{13}	17,559.87	0.0
30	$CH_3 + HO_2 \rightleftharpoons CH_3O + OH$	2.28×10^{13}	0.0	0.0
31	$CH_3 + CHO \rightleftharpoons CH_4 + CO$	3.20×10^{11}	0.0	0.5
32	$CH_3 + CH_3 \rightleftharpoons C_2H_5 + H$	4.90×10^{12}	5,905.41	0.0
33	$CH_4(+M) \rightleftharpoons CH_3 + H(+M)$			
	K_f^0	1.19×10^{35}	53,829.68	−4.911
	K_f^∞	7.05×10^{16}	52,788.95	−0.558
	a^*, b^*, c^*	0.555	405.62	4,580.87
34	$CH_4 + H \rightleftharpoons CH_3 + H_2$	7.80×10^{6}	3,896.85	2.11
35	$CH_4 + O \rightleftharpoons CH_3 + OH$	1.90×10^{9}	4,365.91	1.44
36	$CH_4 + O_2 \rightleftharpoons CH_3 + HO_2$	5.60×10^{12}	28,179.99	0.0
37	$CH_4 + OH \rightleftharpoons CH_3 + H_2O$	1.50×10^{6}	1,226.79	2.13
38	$CH_4 + HO_2 \rightleftharpoons CH_3 + H_2O_2$	4.60×10^{12}	9,056.57	0.0
39	$CH_3O + H \rightleftharpoons CH_2O + H_2$	2.00×10^{13}	0.0	0.0
40	$CH_3O + OH \rightleftharpoons CH_2O + H_2O$	5.00×10^{12}	0.0	0.0
41	$CH_3O + O_2 \rightleftharpoons CH_2O + HO_2$	4.28×10^{-13}	−1,775.23	7.60
42	$CH_3O + M \rightleftharpoons CH_2O + H + M$	1.00×10^{14}	12,628.68	0.0
43	$C_2H_3 + O_2 \rightleftharpoons CH_2O + CHO$	3.98×10^{12}	−120.27	0.0
44	$C_2H_4 + H \rightleftharpoons C_2H_3 + H_2$	3.16×10^{11}	4,029.15	0.70
45	$C_2H_4 + OH \rightleftharpoons C_2H_3 + H_2O$	3.00×10^{13}	1,503.41	0.0
46	$C_2H_5 + H \rightleftharpoons C_2H_4 + H_2$	3.00×10^{13}	0.0	0.0
47	$C_2H_5 + O_2 \rightleftharpoons C_2H_4 + HO_2$	2.00×10^{12}	2,513.71	0.0
48	$C_2H_5(+M) \rightleftharpoons C_2H_4 + H(+M)$			
	K_f^0	6.24×10^{39}	21,384.56	−6.80
	K_f^∞	4.97×10^{10}	18,549.48	0.73
	a^*, b^*, c^*	0.667	653.88	8,733.74
49	$C_2H_6(+M) \rightleftharpoons CH_3 + CH_3(+M)$			
	K_f^0	2.23×10^{61}	49,895.06	−11.992
	K_f^∞	7.10×10^{25}	46,866.83	−2.792
	a^*, b^*, c^*	0.805	302.71	10,730.56
50	$C_2H_6 + H \rightleftharpoons C_2H_5 + H_2$	5.40×10^{2}	2,621.95	3.50
51	$C_2H_6 + OH \rightleftharpoons C_2H_5 + H_2O$	2.20×10^{7}	565.28	1.90
52	$C_2H_6 + CH_3 \rightleftharpoons C_2H_5 + CH_4$	5.50×10^{-1}	4,173.48	4.00

[a]Units are in moles, seconds, centimeters, and Kelvins.
Third-body efficiencies:
(6) $H_2 = 1.9$, $O_2 = 2.6$, $N_2 = 2.6$, $H_2O = 9.5$, $CO = 2.6$, $CO_2 = 2.6$
(12) $H_2 = 2.9$, $O_2 = 1.2$, $N_2 = 1.2$, $H_2O = 18.5$, $CO = 2.1$, $CO_2 = 4.3$
(14) $O_2 = 12.0$, $N_2 = 2.0$, $CO = 3.0$, $CO_2 = 7.0$
(19) $H_2 = 1.87$, $H_2O = 8.12$
(25) $H_2 = 2.9$, $O_2 = 1.2$, $N_2 = 1.2$, $H_2O = 18.5$, $CO = 2.1$, $CO_2 = 4.3$
(42) $H_2 = 2.9$, $O_2 = 1.2$, $N_2 = 1.2$, $H_2O = 18.5$, $CO = 2.1$, $CO_2 = 4.3$

a rod diameter d of 3 and 4 mm. For a rod diameter of 7 mm, the pressure trace clearly showed the presence of combustion.

Figure 1 shows a nondimensional plot of temperature contours for three cylindrical rods having diameters of 1, 3, and 7 mm. A 91 × 91 grid was used, and the flow was assumed to be inviscid. Computations on a 65 × 65 grid yielded similar overall flow features. The results show the advance of the combustion zone, initially constrained to a narrow region near the surface of the smallest rod, toward the bow shock as the diameter of the body is increased. The increase in the amount of combustion as a function of rod size appears to be a continuous process. It should be pointed out that the experiment was designed to determine the diameter of the rod necessary to completely burn the combustible mixture in the test chamber, like in Fig. 1c. However, the experimental setup of Ref. 11 was unable to detect the very small combustion predicted in Fig. 1a, or even the partial combustion predicted in Fig. 1b if the pressure rise occurred downstream of the location of the pressure transducer.

The same computations were conducted by Soetrisno et al.[8] using the quasiglobal combustion model of Westbrook and Dryer.[9] Their computations predict essentially a fully coupled shock-deflagration wave for the same three rod diameters studied here. These results show the inability of the global models to correctly predict the ignition delay. The computation of Soetrisno et al.[8] for a rod diameter of 0.5 mm is comparable to the result presented in Fig. 1c of the present work for a 7-mm-diam cylinder. Neglecting the fact that a somewhat coarser grid was used in Ref. 8 (72 × 65), this indicates that the global model is underpredicting the ignition delay by approximately an order of magnitude.

Figure 2 shows the pressure and temperature variation along the stagnation streamline as a function of the nondimensional distance from the center of the cylinder, x/R (where $R = d/2$) for the three cases. For comparison, the nonreacting solution is also plotted. The shock standoff distance increases with the amount of heat release. The pressure drop behind the shock wave is due to the heat release at subsonic speeds. Figure 3 shows the mole fraction distribution along the stagnation streamline for the 3-mm cylinder. Note that behind the shock, thermal decomposition of CH_4 produces significant amounts of larger hydrocarbons and other radicals within the induction zone. These species then quickly disappear during the heat release process.

These simulations required between 2500–3500 iterations (using a maximum CFL number of ≈8) and between 7–10 h of CPU time on a Cray C90.

The second experiment consisted of a blunt cylinder of diameter d = 7 mm, having its axis aligned with the flow.

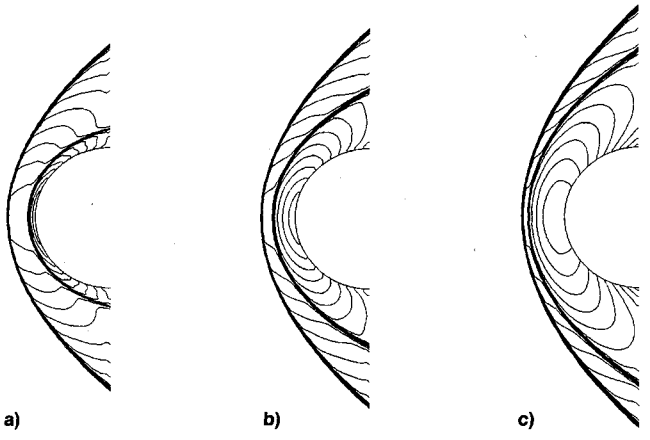

Fig. 1 Nondimensional temperature contours T/T_∞ for three rod diameters and contour values (minimum, maximum, increment): a) d = 1 mm (1.4, 10.6, 0.4); b) d = 3 mm (1.4, 11.0, 0.4); and c) d = 7 mm (1.4, 11.0, 0.4). Stoichiometric CH_4-air; M = 6.61.

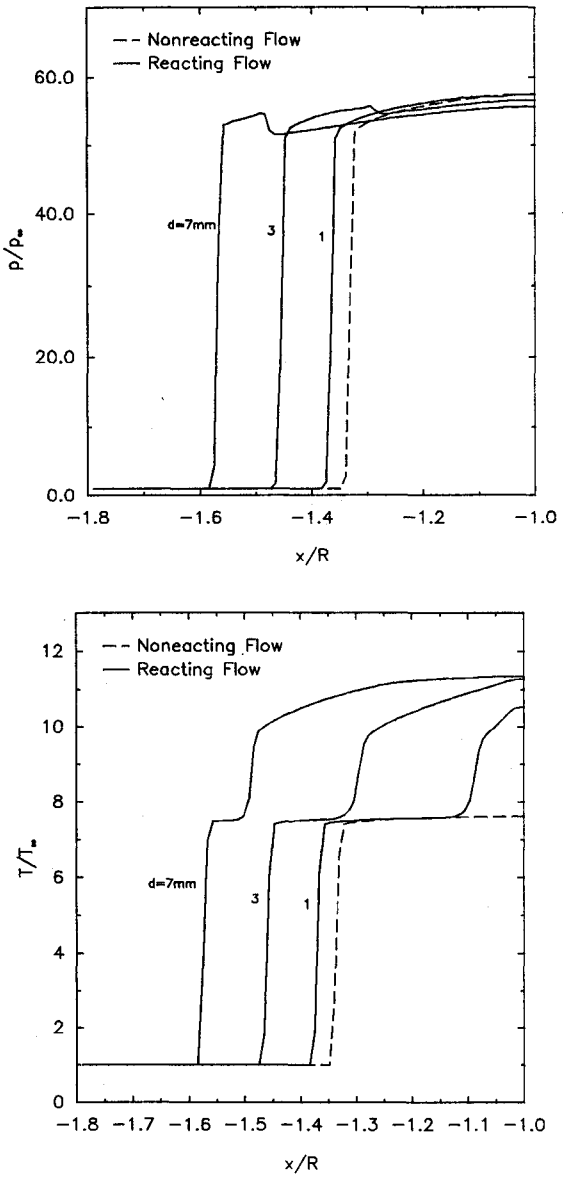

Fig. 2 Pressure and temperature distribution along the stagnation streamline.

The mixture, Mach number, and freestream conditions were identical to the previous case. Calculations assuming viscous, laminar, adiabatic flow were performed on a two-block grid having 75 × 150 and 75 × 91 points. Temperature contours for this case are shown in Fig. 4. The shock and combustion front are separated by a small induction zone. This induction zone widens downstream due to the weakening of the bow shock caused by the expansion waves emanating from the cylinder shoulder. Computations on a 45 × 90 and 45 × 51 grid were too coarse to properly resolve the induction zone, but yielded similar pressure and temperature distribution on the body surface.

This case was also investigated by Soetrisno et al.[8] using several combustion models. Their results indicate also a decoupling of the shock and combustion fronts downstream of the shoulder, however, along the stagnation region, the shock and combustion fronts appear to be fully coupled.

Figure 5 shows the pressure and temperature distribution along the stagnation streamline obtained in the present work, compared with the results of Soetrisno et al. based on the quasiglobal model and a detailed model consisting of 13 species and 19 elementary reactions. All computations give similar pressure distribution with the exception that the von-Neumann spike predicted in the present calculation is not

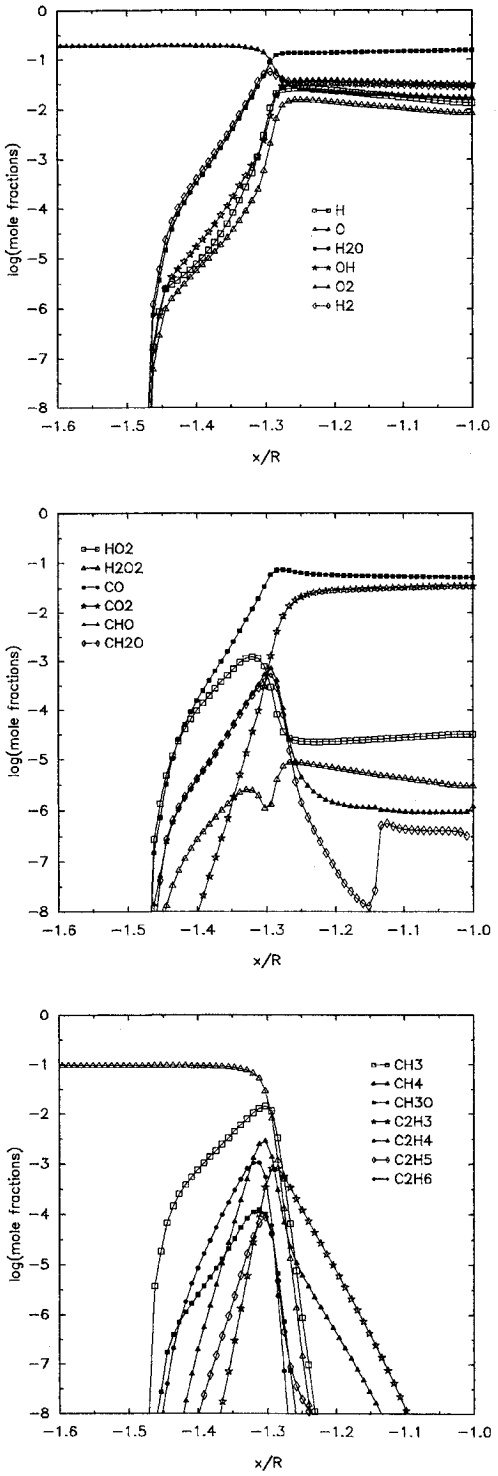

Fig. 3 Concentration profiles along the stagnation streamline; d = 3 mm.

observed in the calculations of Soetrisno et al. The temperature distribution shows significant differences between the two combustion models used in Ref. 8, with the global model showing a better agreement with the present work. Also, the shock standoff distance was slightly larger for the global model than that obtained in the present work.

A quantitative comparison with the interferometry flow visualization of this case presented in Ref. 11 could only be done with respect to the shock standoff distance. A steady combustion process was reported, with a constant shock standoff distance x_{sh}. The experimental value of $x_{sh}/d \approx 0.29$ is in good agreement with the present results and with the full model of Soetrisno et al., both of which predict $x_{sh}/d \approx 0.3$.

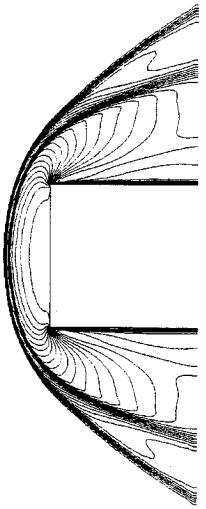

Fig. 4 Nondimensional temperature contours T/T_∞ for a blunt cylinder. Stoichiometric CH_4-air; M = 6.61. Contour values: min = 1.3, max = 11.2, increment = 0.3.

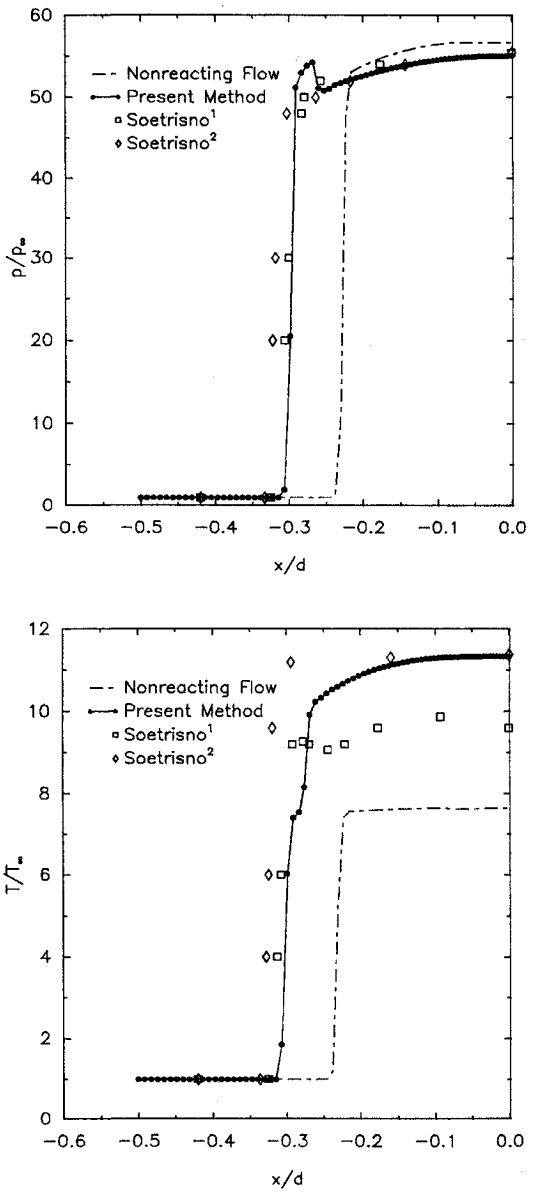

Fig. 5 Pressure and temperature variation along stagnation streamline. Cylinder diameter, d = 7 mm. Soetrisno[1]: detailed 13-species, 19-step model; Soetrisno[2]: quasiglobal model.

Applications to the Ram Accelerator Concept

The ram accelerator is a chemical propulsion method for accelerating projectiles to very high speeds.[6,17] In this device, a shaped projectile is accelerated inside a tube filled with a premixed gaseous fuel/oxidizer mixture. In the high-speed modes of the ram accelerator, ignition is achieved by means of a detonation wave or other forms of shock-induced combustion. Several methods for generating the detonation wave have been proposed. In the simplest method, a series of shock waves reflected from the tube and the projectile surface increase the temperature of the mixture until the ignition temperature is reached at a designed location. The energy released will then establish a detonation wave or a shock-deflagration wave, depending on the mixture composition, pressure and tube size.

In a second method, the forward cone angle of the projectile is kept small to reduce drag and prevent premature combustion, and a detonation wave is generated aerodynamically by inserting a sudden, short axisymmetric ramp[17] with a relatively steep angle, or even a forward facing step as proposed by Rom and Avital[18] in a similar external propulsion accelerator concept. Inviscid simulations of these oblique-detonation-drive concepts, using simple one-step kinetic models, were conducted by Brackett and Bogdanoff[19] and Tivanov and Rom.[20] Accurate prediction of the ignition delay is important for scaling studies, and viscous effects cannot in general be neglected since the boundary layer can interact with the detonation wave and with their shocks to strongly modify the inviscid picture.

In this article, we present first a viscous, laminar flow investigation of the generation of a detonation wave by means of a double ramp using the newly developed methane oxidation mechanism. Then, we incorporate this concept in a ram accelerator configuration.

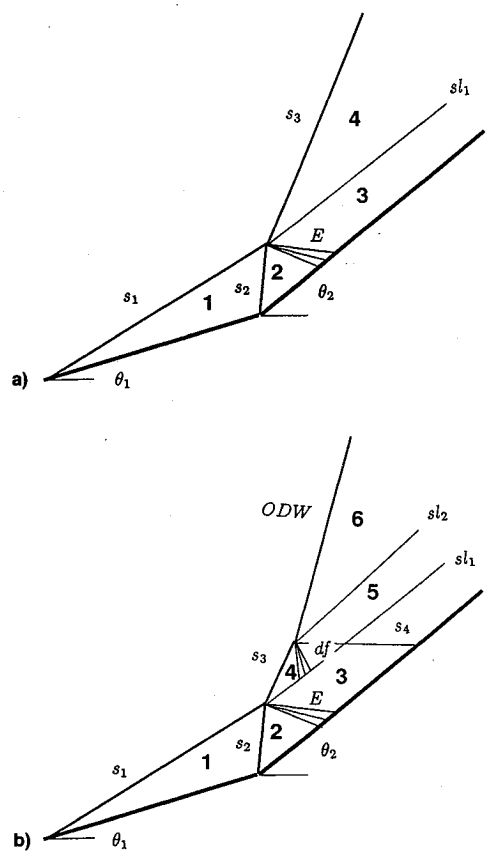

Fig. 6 Schematic of the wave structure on a double ramp for reacting and nonreacting flow. *s*—shock wave; *sl*—slip line; *E*—Prandtl Meyer expansion wave; *df*—deflagration waves; *ODW*—oblique detonation wave: a) nonreacting flow and b) reacting flow.

Figure 6 shows a schematic diagram of the wave structure for nonreacting and reacting flows. In the nonreacting flow case, the two shock waves s_1 and s_2 intersect at point 0. From the intersection point 0, there is a transmitted shock wave s_3 and a weaker wave which, at hypersonic speeds, is always an expansion wave. Regions 3 and 4 in Fig. 6a are separated by a slip line sl_1. The temperature in region 4 is always higher than that of region 3 (except for the boundary layer). This presents the interesting possibility that, for given freestream conditions, ignition is achieved in region 4, but not in region 3. This has the advantage that the detonation wave does not interact directly with the body. However, some combustion can still take place along the boundary layer. This situation, in which region 3 acts as a buffer zone between the detonation wave and the body surface, is illustrated in Fig. 6b. Behind the transmitted shock s_3, there is an induction zone 4, at the end of which energy release becomes significant and generates a set of deflagration waves through which there is a smooth rise in pressure and temperature. These deflagration waves converge into the shock s_3, making it steeper until a new oblique detonation wave and a second slip line are formed. An additional compression wave s_4 is needed to equalize the pressures on the two sides of the slip line sl_2. The flow structure in zones 4, 5, and 6 is similar to that found in a basic detonation on a wedge.[21]

Figure 7 shows temperature contours for nonreacting and reacting flows obtained from a numerical simulation conducted on a double ramp, with $\theta_1 = 18$ deg and $\theta_2 = 36$ deg. The mixture considered is $CH_4 + 4O_2 + 15.04N_2$ (equivalence ratio $\phi = 0.5$). The freestream pressure and temperature are $p_\infty = 1$ atm, $T_\infty = 300$ K, and the Mach number is $M = 7.5$. The computations assumed viscous laminar flow and a constant wall temperature $T_w = 600$ K. The length of the flow domain is 40 cm. Besides the flow structure already described, note that combustion occurs in the boundary layer from the corner of the double ramp and downstream. Because of the reacting boundary layer, a large separation bubble is established at the corner.

Figure 8 shows the pressure and temperature variation along the gridlines $k = 32$, $k = 45$, and $k = 65$. For gridline $k = 32$, the nonreacting plot shows the pressure and temperature jump across the two shocks s_1 and s_2, followed by the expan-

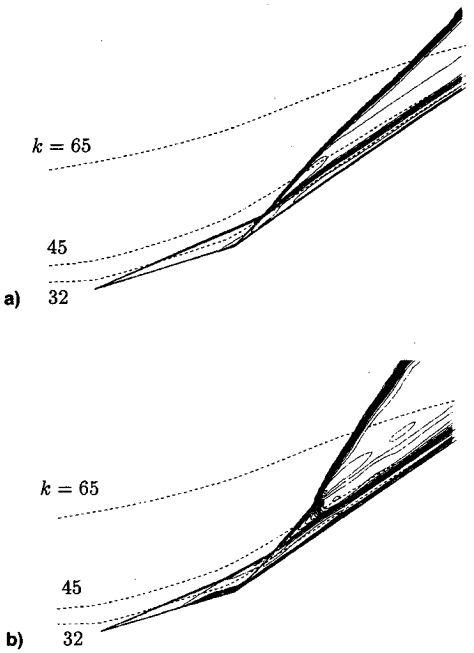

Fig. 7 Nondimensional temperature contours T/T_∞ for a) nonreacting and b) reacting flow past a double ramp. Viscous laminar flow; $M = 7.5$; $\theta_1 = 18$ deg; $\theta_2 = 36$ deg. Contour values (minimum, maximum, increment): a) (1.3, 6.1, 0.3) and b) (1.3, 10.6, 0.3).

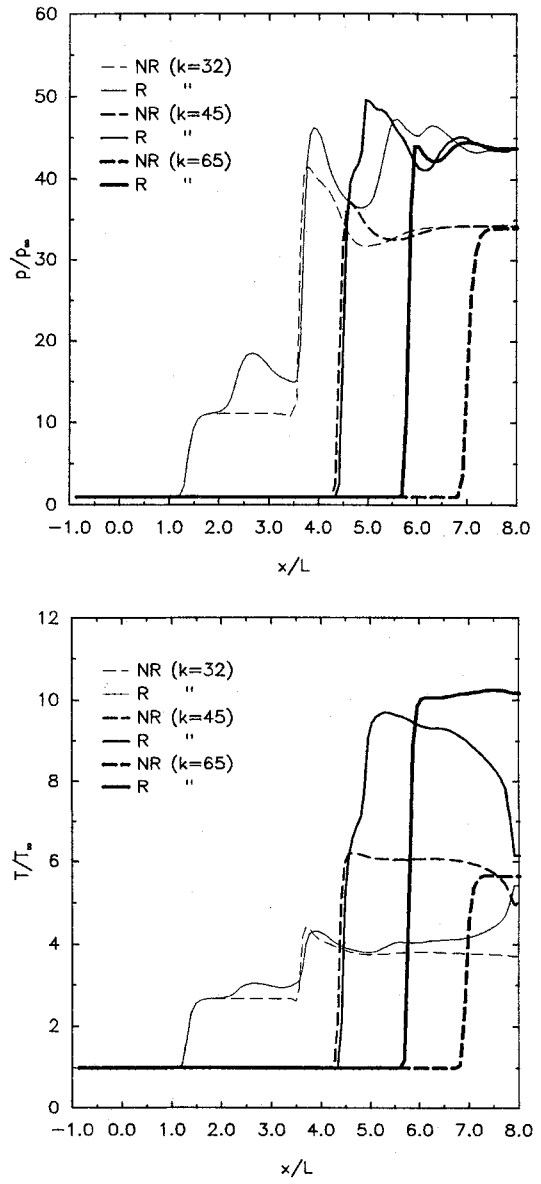

Fig. 8 Pressure and temperature distribution along the three ξ = const grid lines indicated in Fig. 7. NR—nonreacting flow; R—reacting flow. Reference length L = 5 cm.

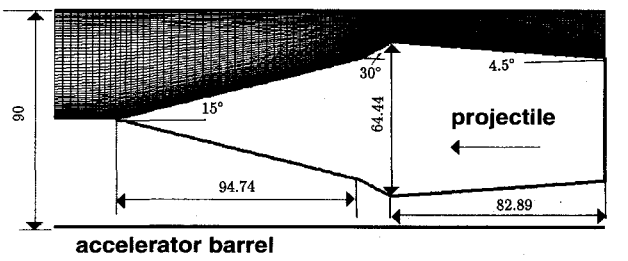

Fig. 9 Schematic of ram accelerator. Grid 195 × 70. Dimensions are in mm.

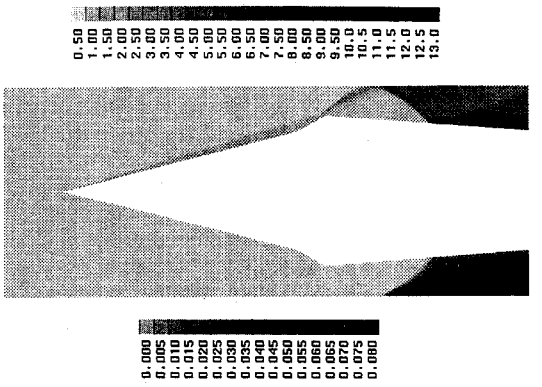

Fig. 10 Nondimensional temperature contours T/T_∞ (top half), and CO_2 mass fraction contours (bottom half). Inviscid M = 9 flow.

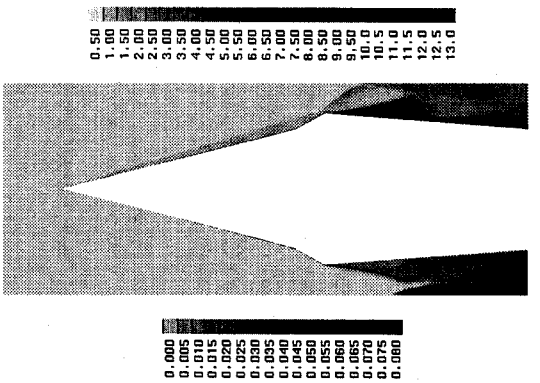

Fig. 11 Nondimensional temperature contours T/T_∞ (top half) and CO_2 mass fraction contours (bottom half). Laminar M = 9 flow.

sion across E. The reacting solution along this gridline shows in addition a jump caused by the separation shock and, behind the expansion, a pressure increase due to combustion. Note that the temperature remains near the nonreacting level except when this gridline crosses the boundary layer and a temperature rise is observed. Along the k = 45 gridline the pressure and temperature show the jump across s_3 followed, in the reacting solution, by a short smooth rise due to the deflagration waves and a final jump caused by the detonation wave. Note that the temperature decreases as the gridline crosses the slip line sl_1. The plot for gridline k = 65 shows the jump across the oblique detonation wave and across s_3 for the reacting and nonreacting cases, respectively. Note in Fig. 8 that in the nonreacting solution, the temperature in region 4 (downstream end of gridline K = 65) is $T_4 \approx 1800$ K, high enough to ignite the mixture, while the temperature in region 3 (downstream end of gridline k = 32) is only $T_3 \approx 1100$ K, too low for ignition. Also note that the pressure at the outflow boundary is basically uniform (as it should be), but that there are large variations in the temperature profile.

The final set of calculations is conducted on an axisymmetric ram accelerator configuration. The geometry is based on a 90-mm tube diam similar to the ISL ram accelerator, and is shown in Fig. 9. The projectile considered has a 15-deg nose cone half-angle, and a 30-deg axisymmetric ramp. The total length of the projectile is 18.95 cm. Although previous inviscid analyses have placed the ramp downstream of the projectile shoulder,[17,19] viscous calculations suggested very strong shock/boundary-layer interactions that completely modified the ideal inviscid flowfield. The projectile configuration considered in the present work is similar to that proposed in Refs. 18 and 20.

Computations were conducted on a 195 × 70 grid for both inviscid and viscous laminar flow. Figures 10 (inviscid) and 11 (viscous) show temperature contours (top half) and CO_2 mass fraction contours (bottom half) for a $CH_4 + 4O_2 + 15.04N_2$ mixture at p_∞ = 1 atm, T_∞ = 300 K, and a Mach number of M = 9. Under these conditions, combustion was initiated by the reflected shock from the tube wall. Steeper cone angles or a scale up of the ram accelerator is required in order for the transmitted shock to ignite the mixture in this case. The adiabatic viscous result (Fig. 11) shows combustion along the boundary layer, and a large separation region behind the projectile shoulder caused by the interaction between the reflected detonation and the reacting boundary layer. Note also that the separated boundary layer affects the manner in which the expansion waves emanating from the projectile shoulder interact with the transmitted shock and with the

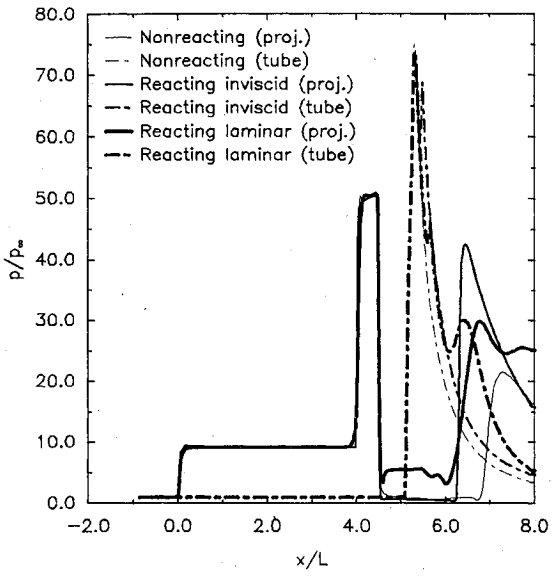

Fig. 12 Pressure distribution along the projectile surface and tube wall; $M = 9$. Reference length $L = 2.3684$ cm.

reflected detonation. The pressure distribution along the projectile surface and tube wall is shown in Fig. 12. The high pressure on the back of the projectile caused by the combustion process can be clearly identified. In the viscous calculation, a small pressure rise occurs immediately behind the projectile shoulder due to the separated boundary layer.

Conclusions

The purpose of this work was to develop the computational tools needed to predict accurately the shock-induced combustion of premixed methane-air hypersonic flows, using a detailed reaction model with as few reactions and species as possible. To accomplish this aim, a new technique, detailed reduction, was employed in developing a combustion mechanism that was accurate over a wide range of conditions and practicable in terms of computational resources. The model was developed for high-speed combustion applications involving lean or rich methane-air mixtures, and should be valid for freestream pressures below approximately 50 atm. However, the model has not been tested at high pressures due to a lack of experimental data in this range. It was demonstrated that previous calculations, based on quasiglobal models, were unable to accurately predict shock-induced combustion flowfields due to their use of severely limited reduced chemical mechanisms. Therefore, the extra cost involved in using the present mechanism is fully justified. It was also shown that a broad range of flow and geometric conditions could be calculated without having to "tune" the chemical mechanism each time. The computational resources needed to tune a mechanism are often greater than those required to run an existing model.

The practical use of the present combustion model was demonstrated for a ram accelerator. A novel double-ramp configuration was investigated. This configuration has the advantage of providing more control over the establishment of the detonation or shock-induced combustion process. In addition, it was shown that a detonation wave could be stabilized without directly interacting with the projectile surface. This could have significant benefits in reducing heat transfer and boundary-layer separation.

Finally, it should be mentioned, that the reaction mechanism presented here could serve as a benchmark against which future, even simpler models could be compared.

References

[1]Frenklach, M., Wang, H., and Rabinowitz, M. J., "Optimization and Analysis of Large Chemical Kinetic Mechanisms Using the Solution Mapping Method-Combustion of Methane," *Progress in Energy and Combustion Science*, Vol. 18, 1992, pp. 47–73.

[2]Westbrook, C. K., and Dryer, F. L., "Chemical Kinetic Modeling of Hydrocarbon Combustion," *Progress in Energy and Combustion Science*, Vol. 10, 1984, pp. 1–57.

[3]Warnatz, J., "Rate Coefficients in the C/H/O System," *Combustion Chemistry*, Springer-Verlag, New York, 1984, Chap. 5.

[4]Miller, J. A., and Bowman, C. T., "Mechanism and Modeling of Nitrogen Chemistry in Combustion," *Progress in Energy and Combustion Science*, Vol. 15, 1989, pp. 287–338.

[5]Sloane, T. M., "Ignition and Flame Propagation Modeling with an Improved Methane Oxidation Mechanism," *Combustion Science and Technology*, Vol. 63, 1989, pp. 287–313.

[6]Hertzberg, A., Bruckner, A. P., and Knowlen, C., "Experimental Investigation of Ram Accelerator Propulsion Modes," *Shock Wave International Journal*, Vol. 1, No. 1, 1991, pp. 17–25.

[7]Nuzca, M., "Numerical Simulation of Reacting Flow in a Thermally Choked Ram Accelerator Projectile Launch System," AIAA Paper 91-2490, June 1991.

[8]Soetrisno, M., Imlay, S. T., and Roberts, D. W., "Numerical Simulations of the Transdetonative Ram Accelerator Combusting Flow Field on a Parallel Computer," AIAA Paper 93-3249, July 1992.

[9]Westbrook, C. K., and Dryer, F. L., "Simplified Reaction Mechanisms for the Oxidation of Hydrocarbon Fuels in Flames," *Combustion Science and Technology*, Vol. 27, 1981, pp. 31–43.

[10]Frenklach, M., "Reduction of Chemical Reaction Models," *Numerical Approaches to Combustion Modeling*, edited by E. S. Oran and J. P. Boris, Vol. 135, Progress in Astronautics and Aeronautics, AIAA, Washington, DC, 1991, Chap. 5.

[11]Srulijes, J., Smeets, G., and Seiler, F., "Expansion Tube Experiments for the Investigation of Ram-Accelerator-Related Combustion and Gasdynamic Problems," AIAA Paper 92-3246, July 1992.

[12]Yungster, S., "Numerical Study of Shock-Wave/Boundary Layer Interactions in Premixed Combustible Gases," *AIAA Journal*, Vol. 30, No. 10, 1992, pp. 2379–2387.

[13]Wang, H., and Frenklach, M., "Detailed Reduction of Reaction Mechanisms for Flame Modeling," *Combustion and Flame*, Vol. 87, 1991, pp. 365–370.

[14]Gordon, S., and McBride, B. J., "Computer Program for Calculation of Complex Chemical Equilibrium Compositions, Rocket Performance, Incident and Reflected Shocks, and Chapman-Jouguet Detonations," NASA SP-273, March 1976.

[15]Shuen, J. S., and Yoon, S., "Numerical Study of Chemically Reacting Flows Using a Lower-Upper Symmetric Successive Overrelaxation Scheme," *AIAA Journal*, Vol. 27, No. 12, 1989, pp. 1752–1760.

[16]Yee, H. C., Klopfer, G. H., and Montagnè, J.-L., "High-Resolution Shock-Capturing Schemes for Inviscid and Viscous Hypersonic Flows," NASA TM-100097, April 1988.

[17]Hertzberg, A., Bruckner, A. P., and Bogdanoff, D. W., "Ram Accelerator: A New Chemical Method for Accelerating Projectiles to Ultrahigh Velocities," *AIAA Journal*, Vol. 26, No. 2, 1988, pp. 195–203.

[18]Rom, J., and Avital, G., "The External Propulsion Accelerator: Scramjet Thrust Without Interaction with Accelerator Barrel," AIAA Paper 92-3717, June 1992.

[19]Brackett, D. C., and Bogdanoff, D. W., "Computational Investigation of Oblique Detonation Ramjet-in-Tube Concepts," *Journal of Propulsion and Power*, Vol. 5, No. 3, 1989, pp. 276–281.

[20]Tivanov, G., and Rom, J., "Investigation of Hypersonic Flow of a Detonable Gas Mixture Ahead of a Forward Facing Step," AIAA Paper 93-0611, Jan. 1993.

[21]Li, C., Kailasanath, K., and Oran, E. S., "Effects of Boundary Layers on Oblique-Detonation Structures," AIAA Paper 93-0450, Jan. 1993.